CHAPTER IV
RESULTS AND DISCUSSION

4.1 Cross-linked Chitosan Beads (CCB)

The chitosan beads both original gel beads and cross-linked beads prepared as described in the previous chapter had a spherical structure and a diameter of around 3 mm. Figures 4.1 and 4.2 show the pictures of chitosan beads before and after cross- linking, respectively. It should be noted that the effect of the concentration of chitosan and NaOH in the casting solution on physical properties of the chitosan beads was observed during the preparation of the chitosan beads. The changes in pore size, porosity and diameter of the chitosan beads have previously been reported (Kawamura *et al.*, 1997). After a few trials, the concentrations of chitosan and NaOH were set at 2 w/v% and 2 M, respectively. Under this specific condition and fixed stirring speed (500 rpm), the spherical chitosan beads with uniform size and shape could be obtained.

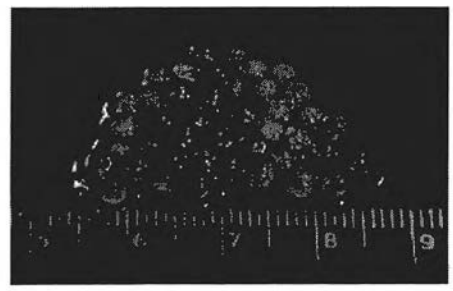

Figure 4.1 Chitosan gel-beads after washing from precipitation bath.

Figure 4.2 Cross-linked chitosan beads (CCB).

The acid tolerance and mechanical strength of the chitosan gel beads formed can be further improved by cross-linking. The CCB had been shown to possess superior mechanical strength and acid tolerance as compared to the original gel beads (Guibal et al., 1998; Juang and Ju, 1998). It was observed in this work that the uncross-linked beads were easily broken upon being agitated by a magnetic stir bar in a beaker while the cross-linked ones appeared to be undamaged at all. For acid tolerance testing, a comparative study was conducted by suspending the cross-linked and uncross-linked beads in an acidic solution of pH 2 for the same period of time. The uncross-linked beads were dissolved quickly in this acidic solution whereas there was no change observed in case of the cross-linked ones. However, it is worth mentioning that despite the enhancement of acidic durability and mechanical strength properties of the chitosan beads by cross-linking, this may reduce the crushing strength and the elastic properties of chitosan gel-beads by shifting the void fraction from macropores to mesopores as the internal surface area increased (Hsien and Rorrer, 1995). In other words, chitosan beads may become more brittle after cross-linking as a result from the interaction between dialdehyde group (-COH) on glutaraldehyde and amine group ($-NH_2$) on chitosan which may reduce the elasticity of linear chitosan polymer chain. Hence, the concentration of glutaraldehyde and the ratio between glutaraldehyde solution and gel beads were the important factors to maintain the mechanical property of cross-linked beads during the adsorption. Cross-linking time was also the one of the factors which can control the brittleness of cross-linked beads. The usage of 1 v/v% glutaraldehyde aqueous solution at the ratio of 15 ml: 1 g. touch-dried beads with a gentle stirring for 10 hours appeared to be the appropriate conditions for the system used in this study.

(a)

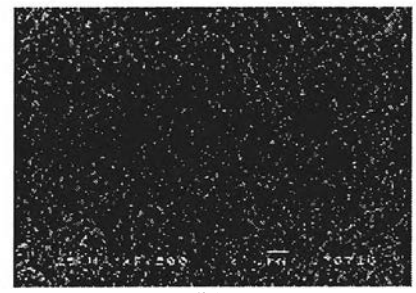

(b)

Figure 4.3 Scanning electron micrographs of the CCB.

Figure 4.3(a) shows the electron micrograph of the CCB. Figure 4.3(b) shows the cross-sectional view of the bead shown in Figure 4.3(a) at 7,500 magnifications. It can be seen that the CCB had high porosity. These beads had no the so-called skin-core structure, indicating that the solidifying agent, NaOH, can diffuse throughout the chitosan gel-beads and into the center of the particles during the cross-linking step. Furthermore, the BET results report that the surface area of the CCB was around 30 m^2/g of dried bead.

4.2 Adsorption of Reactive Red 180

4.2.1 Adsorption Kinetics

The adsorption kinetics of reactive dye RR180 by the CCB had been studied in batch mode of operation under various conditions. Figure 4.4 shows the kinetic data of the adsorption of dye by the CCB in the batch liquid adsorption experiment with the initial RR180 dye concentration of 200 mg/L and at pH values of 2, 4, 6, and 8.

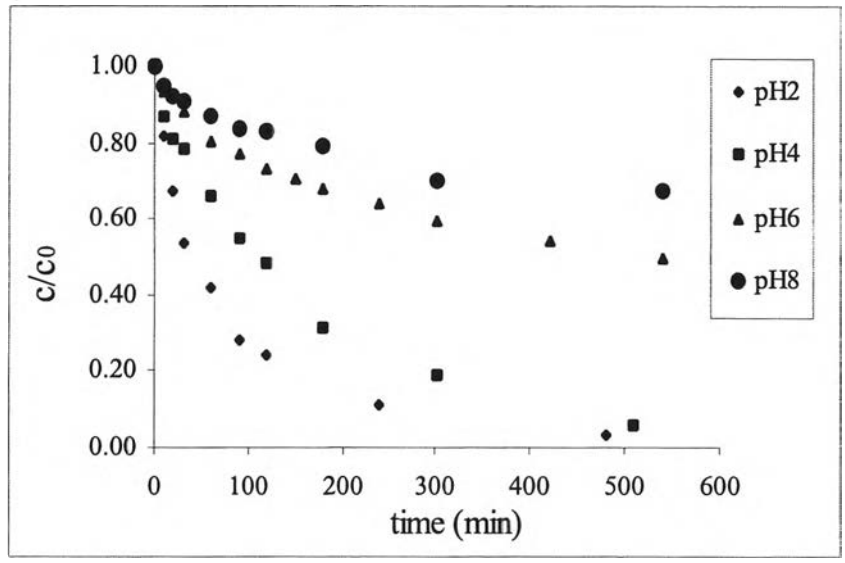

Figure 4.4 Kinetic of RR180 adsorption by the CCB (c_0 = 200 mg/L) at various pH values.

It can be seen from Figure 4.4 that the adsorption of dye by the CCB was rapid during the first couple of hours. The adsorption continued for several hours at much slower rate and reached equilibrium at approximately 10 h. or 600 min. This figure shows that the adsorption of reactive dye RR180 increased with decreasing pH of the solution. Adsorption of dye by the CCB at pH 2 had shown to be much higher than the adsorption at pH 4, 6 and 8, respectively. This can be explained by the fact that upon lowering pH of the solution, the amine groups in chitosan beads became more protonated, thus leading to higher dye adsorption.

The adsorption capacity (q, mg/g adsorbent) can be calculated from the kinetic data in Figure 4.4, by mass balance of the initial concentration and the supernatant concentration at corresponding time interval. Consequently, the adsorption capacity, q, can be plotted as a function of time in various forms (e.g., $t^{1/2}$, ln t, etc.) in order to investigate the process controlling the adsorption of dye by the CCB. Three diffusion models: pseudo first order, pseudo second order and particle diffusion have been used to fit with the kinetic data. It was found that the adsorption behavior of RR180 sorption by the CCB was best described by the particle diffusion model as shown in Figure 4.5, in which the adsorption capacity (q) was plotted

against square root of time ($t^{0.5}$). A linear correlation obtained from the experimental results revealed that particle diffusion was the dominant mechanism controlling the adsorption of RR180 dye by the CCB (Juang and Ju, 1998).

Previous studies showed that such a plot may present a multilinearity (Guibal *et al.*, 1995; Juang *et al.*, 1997; Juang and Ju, 1998). This indicated that two or more phenomena occurred successively. In general, this tendency can be divided in to 3 parts. The first portion represented the external surface adsorption, which was controlled by external diffusion between solute in the solution to the thin film layer. The second portion was the gradual adsorption which was controlled by intraparticle diffusion, and the last portion was the final stage adsorption which occurred when the system reached the equilibrium or low solute concentration. The first linear portion can become negligible if adequately high stirring rate was used as observed in this study. It was seen from Fig. 4.5 that the second, gradual linear, portion was the dominant portion of the curve. The third linear portion was observed after approximately 600 min (or 10 h.), which indicated the time when equilibrium was reached. This clearly demonstrated that the intraparticle diffusion was the rate-limiting step in the sorption kinetics of reactive dye RR180 on the CCB. Similar results were also observed by Wu et al. (1999).

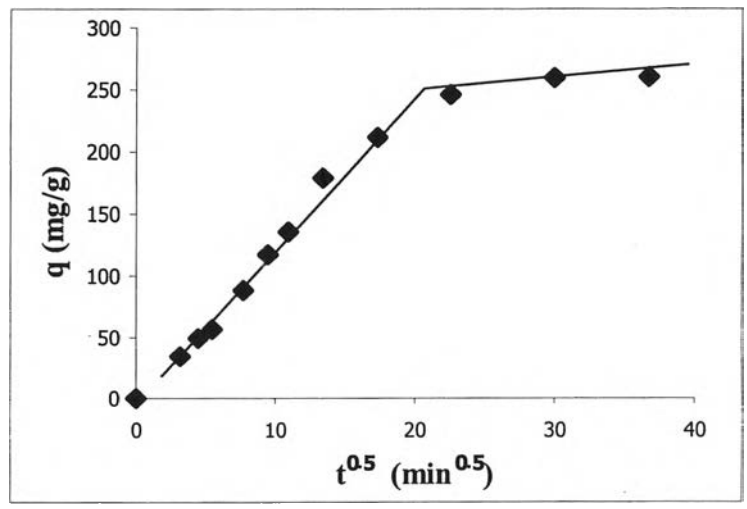

Figure 4.5 Test of the intraparticle diffusion model for the adsorption of RR180 dye on the CCB at pH 4.

4.2.2 Adsorption Isotherms

From the equilibrium adsorption experiments under ambient condition, the adsorption isotherms of reactive dye RR180 on the CCB at four different pH (2, 4, 6 and 8) were constructed as shown in Figure 4.6. As clearly shown in the previous section, the experiments for equilibrium adsorption in this section were carried out for at least 24 h. to assure that the equilibrium was reached before any measurements were taken. Initially, the equilibrium data were fitted with both Langmuir and Freundlich isotherms. It was found that the data were best fitted with the Langmuir isotherm which can be written as:

$$q_e = \frac{q \times c_e}{K_L + c_e} \qquad (1)$$

Where q_e and c_e are the total amount of dye adsorbed on the CCB and the total dye concentration remained in solution at equilibrium, respectively. After linearization, Langmuir affinity constant (K_L) and maximum monolayer adsorption capacity corresponding to complete monolayer coverage (q) can be determined. The affinity constant and the maximum adsorption capacity from pH 2-8 were summarized in Table 4.1. The adsorption of RR180 has a strong pH-dependent characteristic as expressed by Figure 4.7. The much higher adsorption of dye at lower pH observed in this figure agreed well with the results obtained from the kinetic studies (Figure 4.4).

Similar explanation could be offered as more amine sites were protonated at lower pH. The adsorbed amount observed in the present study was significantly greater than those obtained in the previous studies on dye adsorption using other natural and natural-based adsorbents such as activated carbon, clay minerals, bagasse, maize cob both in terms of capacity and affinity (McKay, 1982; El-Geundi, 1991).

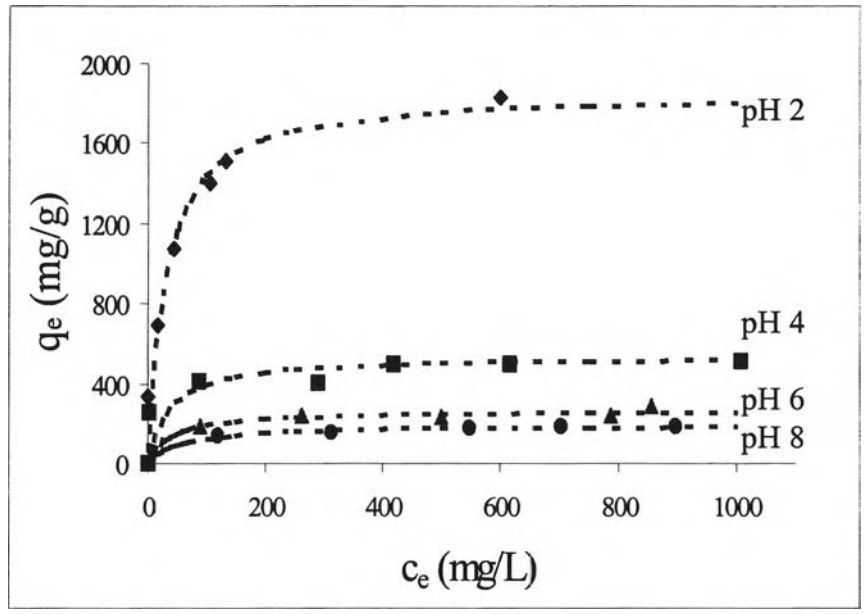

Figure 4.6 Adsorption isotherms for RR180 removal using the CCB at pH 4 and 6. Lines shown are curve-fitting by Langmuir model.

Table 4.1 Maximum monolayer adsorption capacity (Q), Langmuir affinity (K_L) and initial adsorption rate of RR180 adsorption at pH 2-8

pH	Max. monolayer adsorption capacity (Q) mg/g	Langmuir affinity (K_L) mg/L	Initial Ads. Rate (mg/g*min)
2	1856	28.76	3.61
4	540	35.83	2.17
6	270	39.70	1.19
8	196	56.43	0.91

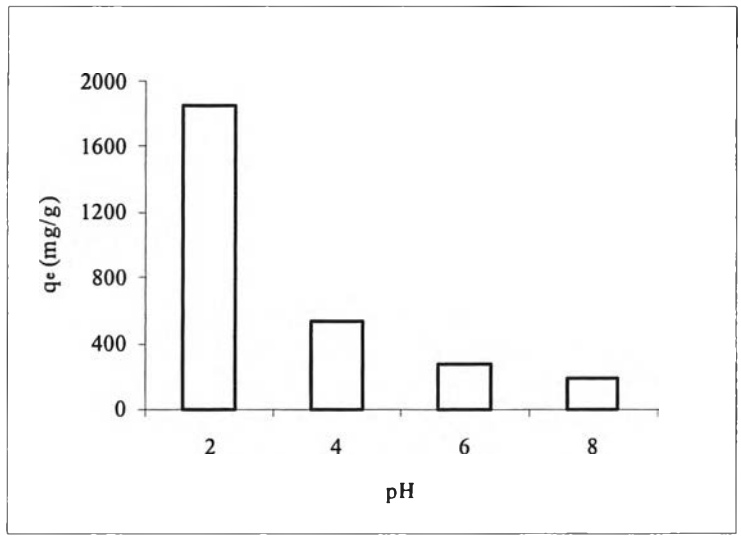

Figure 4.7 Effect of pH on the adsorption of RR180 on CCB.

4.3 Adsorption of Heavy Metal

4.3.1 Adsorption Kinetics

Using Cu^{2+} aqueous solution as model waste metal ions, adsorption of Cu^{2+} by the CCB was conducted in batch mode. For all experiments, the initial concentration of Cu^{2+} ion was fixed at 100 mg/L, which was quite similar to the level in the textile wastes stream. The procedures were the same as used in the dye adsorption. Figure 4.8 shows the kinetic data of Cu^{2+} adsorption on the CCB at pH 2 and 4. The precipitation of Cu^{2+} as metal hydroxides was noticed when pH of the system rose up to 6 and 8. Hence, all Cu^{2+} adsorption experiments were carried out only at pH 2 and 4, both in single- and mixed-ion systems.

Similar to RR180, Cu^{2+} ions were rapidly adsorbed on the CCB during the first few minutes before the equilibrium was reached within approximately 10 hours. Once again the intraparticle diffusion model was used to describe the adsorption controlling step. The two linear portions were observed as shown in Figure 4.9. According to the repulsion between two positively charge molecules, the protonated amine groups ($-NH_3^+$) and copper cations (Cu^{2+}), the lower pH provided a stronger repulsion, which inhibited the adsorption of Cu^{2+} onto CCB.

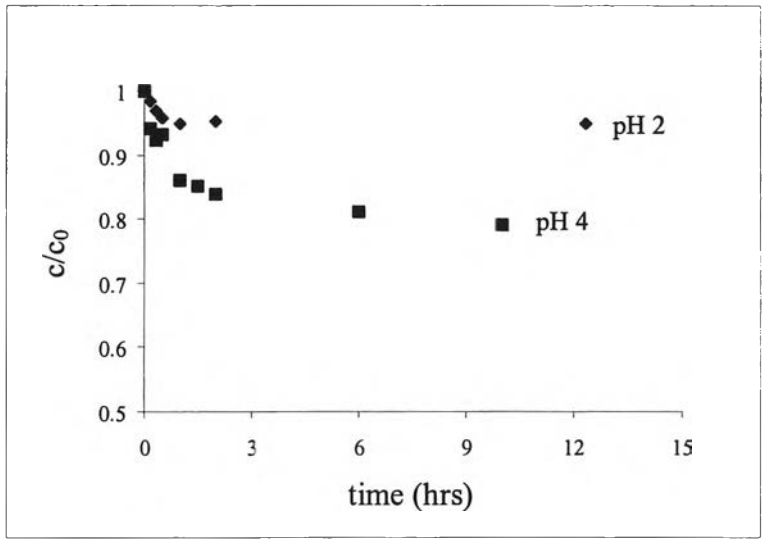

Figure 4.8 Kinetic of Cu^{2+} adsorption by the CCB (c_0 = 100 mg/L) at pH 2 and 4.

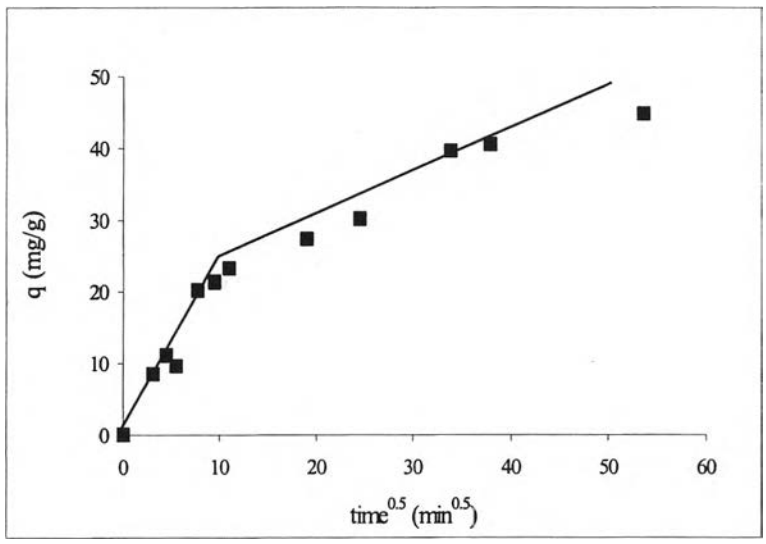

Figure 4.9 Test of the intraparticle diffusion model for the adsorption of Cu^{2+} on the CCB at pH 4.

Lee *et al.* (2001) proposed two possible mechanisms for heavy metal chelating by deacetylated chitin, i.e. ion-exchange mechanism and complexation mechanism. They concluded that the adsorption of Cu^{2+} preferred to form a complex with hydroxyl (-OH) and amine ($-NH_2$) functional groups than exchanging with the protonated amine groups ($-NH_3^+$). In this study, the change in colour of copper ions

from blue in fresh aqueous solution to green upon adsorbing on CCB was observed, suggesting that the adsorption of copper ions was through the complexation mechanism rather than a simple ion-exchange mechanism.

4.3.2 Adsorption Isotherms

Cu^{2+} adsorption isotherms were constructed in a similar manner as the RR180 adsorption isotherms. The system was left over 24 hours in order to make sure that equilibrium was achieved before any further quantitative analysis was made. Figure 4.10 demonstrates the adsorption isotherms of Cu^{2+} on the CCB. The Cu^{2+} adsorption was also exhibited a Langmuir-type isotherm. After linearization, the Langmuir affinity (K_L) at pH 2 and 4 were determined to be 523.1 and 86.46 mg/L, respectively, whereas the maximum monolayer adsorption capacity (q) at pH 2 and 4 were 54.05 and 89.98 mg/g, respectively.

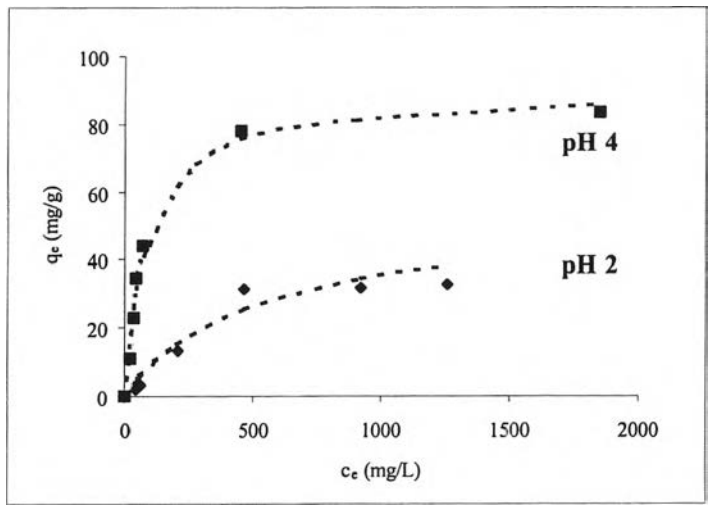

Figure 4.10 Adsorption isotherms for Cu^{2+} removal using the CCB: Experimental data and modeled curves (dashed line: Langmuir model) for pH 2 and 4.

4.4 Adsorption of Reactive Dye and Heavy Metal in Mixed-Ion Systems

4.4.1 Adsorption Kinetics

The adsorption of mixed-ion system of reactive dye and heavy metal was carried out using a fixed molar ratio between RR180 and Cu^{2+} ions of 1:1. In terms of analysis, it was found that RR180 and Cu^{2+} ions had no interference to each other in mixed-ion system. From the kinetic data shown in Figures 4.11 and 4.12, the adsorption behavior had the same tendency as in the single-ion adsorption. The adsorption of both RR180 and Cu^{2+} ions onto CCB in mixed-ion system occurred quite fast at the first period of time before reaching equilibrium. Similarly, the internal diffusion was shown to be the controlling step in the adsorption. The intraparticle diffusion model also exhibited two linear portions as seen in the single-ion system. Explanation can be offered here as described in the previous sections. The adsorption of RR180 was driven by electrostatic force between the protonated amine groups inside chitosan structure and dye anion molecules whereas the adsorption of Cu^{2+} has shown to be through complexation mechanism with the amine groups.

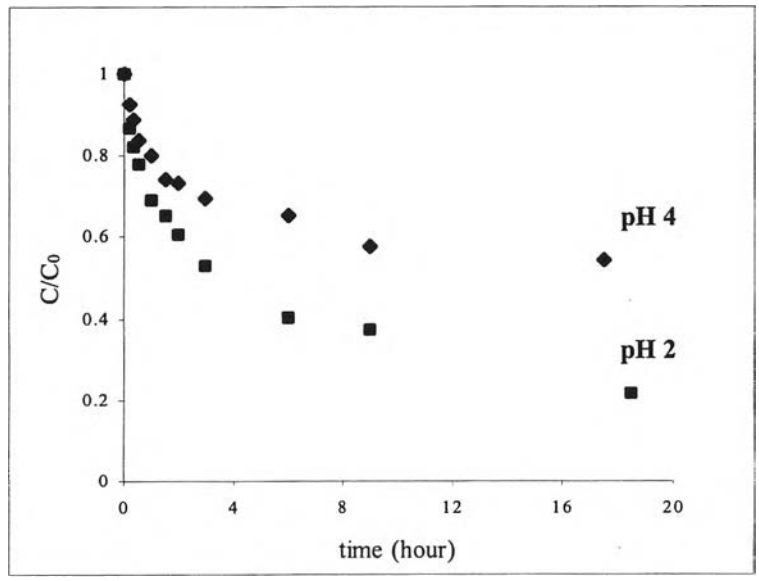

Figure 4.11 Kinetic of RR180 adsorption on the CCB in mixed-ion system at pH 2 and 4 (C_0 = 1000 mg/L).

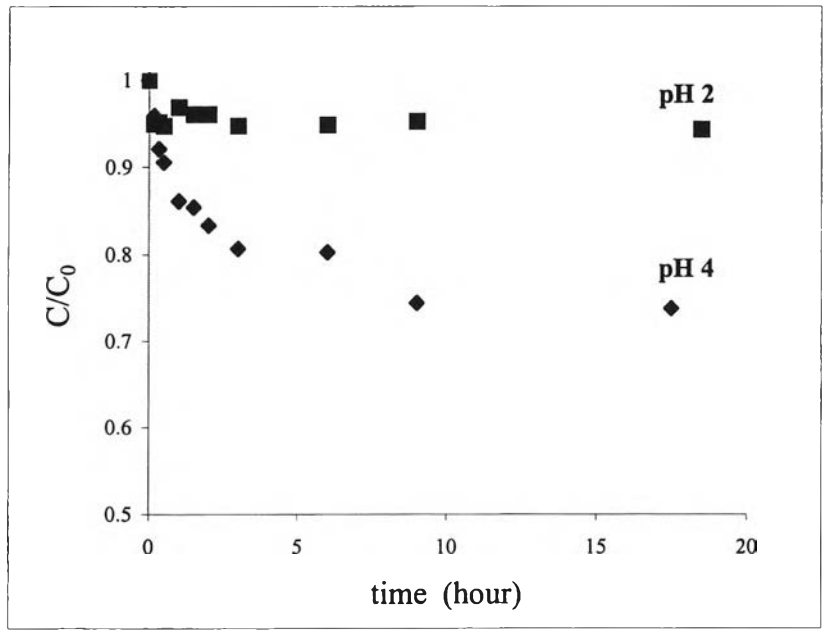

Figure 4.12 Kinetic of Cu^{2+} adsorption on the CCB in mixed-ion system at pH 2 and 4 (C_0 = 100 mg/L).

4.4.2 Adsorption Isotherms

The comparison of the adsorption isotherms of RR180 and Cu^{2+} between the single-ion system and mixed-ion system are shown in Figures 4.13 and 4.14, respectively. Similar to the single-ion equilibrium adsorption, Langmuir adsorption isotherm offered the best fit with the equilibrium adsorption data of the mixed-ion systems. As a result, the maximum adsorption capacity (q) and the Langmuir affinity (K_L) could be determined from this Langmuir equation so as to evaluate the sorption characteristics of CCB in mixed-ion systems. The values are summarized in Table 4.2. The results clearly show that the adsorption of RR180 and Cu^{2+} on CCB in mixed-ion system also had the same pH-dependent characteristic as observed in the single-ion system.

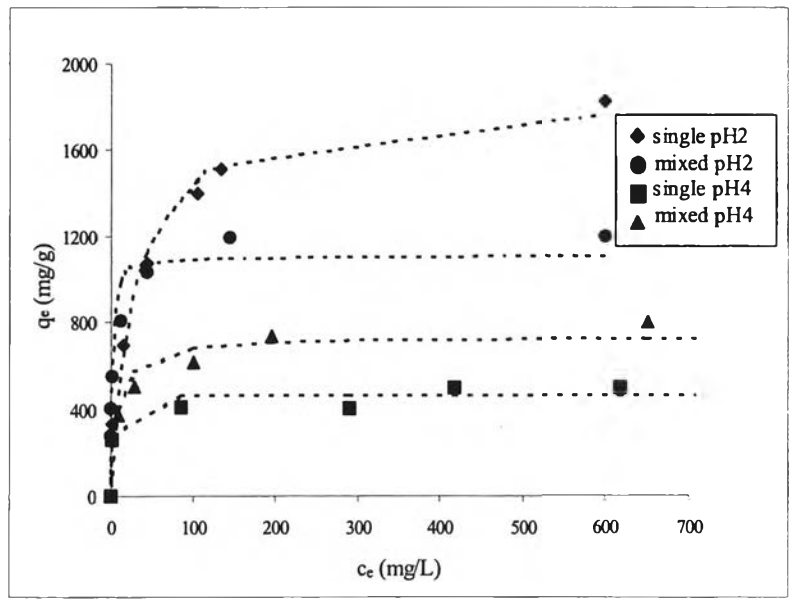

Figure 4.13 Comparison of RR180 adsorption isotherms of single- and mixed-ion systems at pH 2 and 4.

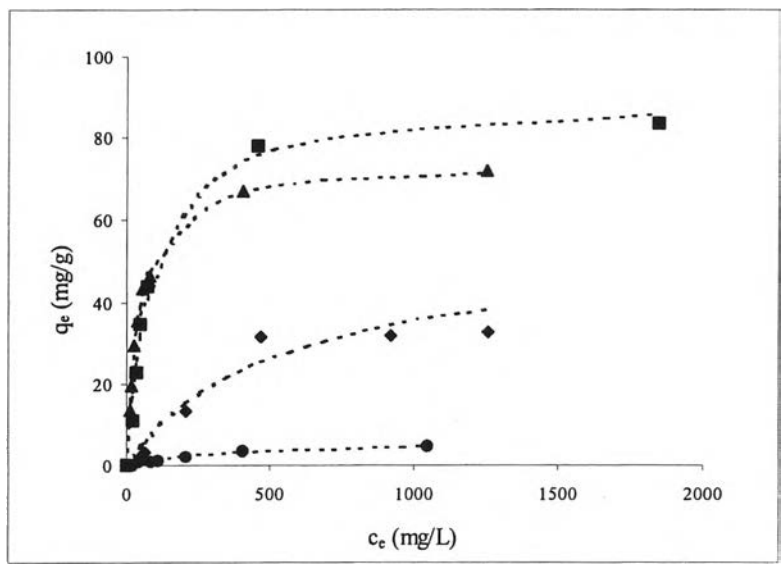

Figure 4.14 Comparison of Cu^{2+} adsorption isotherms of single- and mixed-ion systems at pH 2 and 4 (using the same symbols in Figure 4.13).

Table 4.2 Maximum monolayer adsorption capacity (Q), Langmuir affinity (K_L) and initial adsorption rate of both single- and mixed-ion system at pH 2-8

System	pH	Max. monolayer adsorption capacity (Q) mg/g	Langmuir affinity (K_L) mg/L	Initial Ads. Rate (mg/g*min)
Single RR180	2	1856	28.76	3.61
	4	540	35.83	2.17
Single Cu^{2+}	2	54.05	523.1	0.23
	4	89.98	86.46	0.61
Mixed RR180	2	1110	1.45	11.67
	4	734	7.84	8.59
Mixed Cu^{2+}	2	6.33	371.8	0.35
	4	74.02	43.51	0.56

From the above results, the comparison of RR180 and Cu^{2+} adsorption between single- and mixed-ion systems can be done. The competitive effect on the adsorption of RR180 and Cu^{2+} ions by CCB should be investigated in mixed-ion system since both RR180 and Cu^{2+} ions may be adsorbed onto the same active sites on CCB. Mostly, the adsorption capacity in single-ion system was greater than mixed-ion system except the adsorption of RR180 at pH 4 as shown in Figures 4.13 and 4.14. For dye adsorption, the adsorption capacity at pH 2 was obviously higher than that obtained in the single-ion system, suggesting that the competitive effect from Cu^{2+} was not significant. It should be noted that relatively small amount of Cu^{2+} was adsorbed on CCB in mixed-ion system at this pH, thus having only little impact on RR180 adsorption. In contrast, at pH 4 where a much higher amount of Cu^{2+} was adsorbed, the adsorption capacity in mixed-ion system was greater than that observed in the single-ion system. The results suggested that the presence of Cu^{2+} in mixed-ion system might contribute to the increase in RR180 binding. The small and simple Cu^{2+} molecules can diffuse through the internal pores inside CCB more rapidly than complex molecules of RR180. At the same time as complexation were formed, Cu^{2+}

molecules can induce the RR180 anions by electrostatic force forming the coordination linkage between active amine sites, Cu^{2+} molecules and RR180 anions. Similar explanation was also offered by Shimizu *et al.* (1995). They observed that the presence of heavy metal, i.e. Co^{2+} and Cu^{2+} might promote the adsorption of violet chrome, the acid azo dye, onto the partially deacetylated chitin polymer. The formation of polymer-metal-dye complexation behavior was ascribed as well.

4.5 Column Operation

After the batch adsorption studies, a preliminary study on the adsorption of RR180 and Cu^{2+} by CCB in a column operation was conducted to evaluate the possibility for using the CCB in a continuous removal of textile waste containing dye and heavy metal. The column studies were conducted in a glass column (1.6cm ID, 10 cm height) filled with the CCB as a fixed-bed adsorber. A solution containing RR180 or Cu^{2+} was pumped through this adsorption column in downflow direction, and the effluent stream was drawn out at the column exit for further analysis. After a few trials, the column was operated at the volumetric flow rate of 1 ml/min for and an initial concentration of RR180 and Cu^{2+} were 5 and 10 ppm at pH 4, respectively. The breakthrough curves of the dye and Cu^{2+} adsorption are shown in Figures 4.15 and 4.16, respectively. Due to the low adsorption rate as previously observed in batch adsorption studies (Figures 4.4 and 4.8), the separation of both contaminants required a long time to obtain a complete breakthrough curve. When comparing dye and metal adsorption (Figures 4.15 and 4.16), we found that the adsorption of RR180 required much longer time to complete the breakthrough curve. This can be explained that the molar adsorption rate of RR180 was slower than the molar adsorption rate of Cu^{2+} as seen in the previous section (Figures 4.11 and 4.12). Since it has been shown that the adsorption of both RR180 and Cu^{2+} was controlled by the intraparticle diffusion (Figures 4.5 and 4.9), it should be more difficult for RR180, being much larger molecule than Cu^{2+}, to diffuse through CCB and get adsorbed on the active sites, thus requiring much longer time to reach full adsorption capacity of the column.

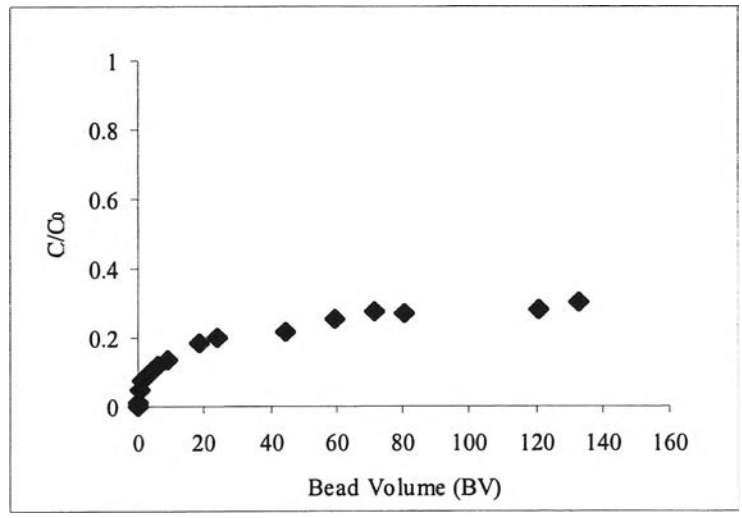

Figure 4.15 Breakthrough curve of RR180 removal (C_0 = 5 ppm, v_0 = 1 ml/min, pH 4).

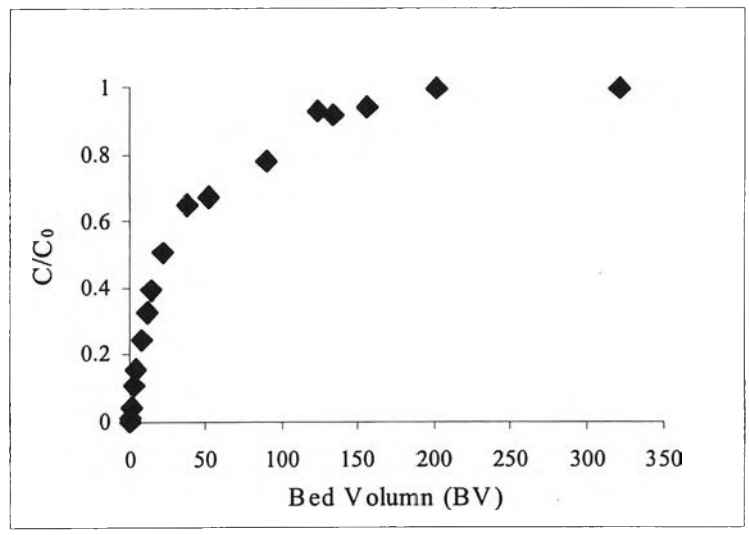

Figure 4.16 Breakthrough curve of Cu^{2+} removal (C_0 = 10 ppm, v_0 = 1 ml/min, pH 4).